# Wireless Temperature Monitoring With Shape Memory Alloy-Based Antenna

Wei Wang <sup>10</sup>, Wenxin Zeng, Aydin Sadeqi <sup>10</sup>, and Sameer Sonkusale <sup>10</sup>

Abstract—Economical sensing and recording of temperature are important in the transportation and management of fragile goods such as medicine, fish/poultry, and other temperature-sensitive items. Existing approaches measure the entire temperature profile using electronic devices running on a continuous power source. This letter presents a simple, intelligent, and battery-free solution for capturing interesting temperature events using the natural thermomechanical state of a shape memory alloy (SMA). Our approach utilizes the temperature variation induced irreversible configuration of SMA, which provides a natural ability to capture the temperature history without the need for electronic data logging. In this letter, SMA is used to record the threshold temperature violation event. A prototype antenna is shown to monitor the temperature at 30 °C with a ±1 °C error. A difference of 17 dB in frequency response was observed with and without temperature violation. Detailed design and experimental studies have been performed to validate the proposed approach.

Index Terms—Shape memory alloy (SMA), temperature recording, temperature sensing.

## I. INTRODUCTION

HERE is a need to develop low-cost wireless temperature sensors to monitor fragile goods during transit and handling [1]. For instance, certain drugs and chemicals must be stored under a given temperature to ensure viability. Additionally, perishable food (e.g., fruits and vegetables) may need to be stored at an optimal temperature to ensure freshness and quality. In these applications, temperature sensors that can record critical temperature violation events are essential. While one can employ an active temperature sensor to continuously record the entire temperature history during transit, this requires electronic memory, associated electronics, and a dedicated battery or wireless energy harvest circuit making this cost-prohibitive except for the most expensive goods. A simple low-cost device that monitors and records critical temperature violations will enable transit chain visibility for many temperature-sensitive items at a fraction of the cost of today's solutions.

A brief review of temperature sensors ranges from resistance temperature detectors (RTD), thermocouple, to chip-based thermometer. RTD is based on the temperature-dependent resistivity

Manuscript received November 10, 2020; revised December 10, 2020; accepted December 28, 2020. Date of publication January 1, 2021; date of current version March 3, 2021. This work was supported by National Science Foundation 1808912. (Corresponding author: Sameer Sonkusale.)

Wei Wang was with the Nano Lab, Department of Electrical and Computer Engineering, Tufts University, Medford, MA 02155 USA. He is now with Analog Devices, Colorado Springs, CO 80920 USA (e-mail: wei.wang@tufts.edu).

Wenxin Zeng, Aydin Sadeqi, and Sameer Sonkusale are with the Nano Lab, Department of Electrical and Computer Engineering, Tufts University, Medford, MA 02155 USA (e-mail: wenxin.zeng@tufts.edu; aydin.sadeqi@tufts.edu; sameer@ece.tufts.edu).

Digital Object Identifier 10.1109/LAWP.2020.3048884

of a material [2]. The thermocouples use the thermoelectric effect where a thermal gradient generates a small voltage on the metal-metal junction [3]. Most integrated chip-based temperature sensor chips operate by measuring the base-emitter voltage of a bipolar transistor, which depends on temperature [4]. Temperature-sensitive materials have also been applied to the resonant circuit to perform sensing functions with wireless communication capability. For example, the shift in the resonant frequency due to changes in the temperature-sensitive material have been demonstrated [5]–[7]. Nevertheless, existing methods require continuous measurement and storage of the entire temperature record using power-hungry electronic devices to find any critical violations.

With the expansion of sensors in the Internet of Things, low-power consumption has become one key feature of the sensors. For example, threshold temperature sensor [8], peak temperature sensor [9], package opening sensor [10], [11], and security sensor [12] have been developed. Relying on the material properties, these sensors detect and record the interested events without any power sources. However, these sensors are designed for single use only. Development of reusable zero-power sensors could further reduce the cost.

In this letter, we present an economical battery-free threshold temperature sensing and recording approach using shape memory alloy (SMA). In the realization, SMA is assembled as arms of temperature-sensitive antennas without the need for any other components. Exceeding a temperature threshold causes the antenna to irreversibly change (deform) its configuration, which alters its radiation profile. This temperature-crossing event could be detected using a radio frequency reader at any time point following the event. The sensor itself operates without the need for power resources, which greatly reduces the cost and makes this platform scalable for tracking many goods.

# II. BACKGROUND ON SMAS

SMAs are metal alloys with intrinsic thermo-mechanical memory and exist in the austenite phase and the martensite phase. With an increase in temperature, an SMA converts from a martensite phase to an austenite phase; reversely, with a decrease in temperature, the SMA converts back from an austenite phase to a martensite phase as in Fig. 1. The critical start and end temperature in the formation of the martensite phase and austenite phase are defined as Ms, Mf, As, and Af, respectively. SMA has three crystal structures (austenite, twinned martensite, and detwinned martensite) as indicated in Fig. 2. At high temperatures, the SMA is in a stable austenite phase where the atoms are

1536-1225 © 2021 IEEE. Personal use is permitted, but republication/redistribution requires IEEE permission. See https://www.ieee.org/publications/rights/index.html for more information.

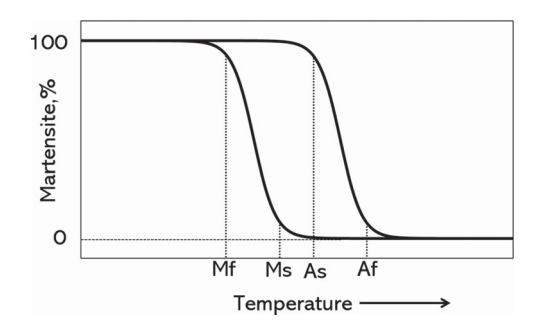


Fig. 1. Critical temperatures in phase conversion.

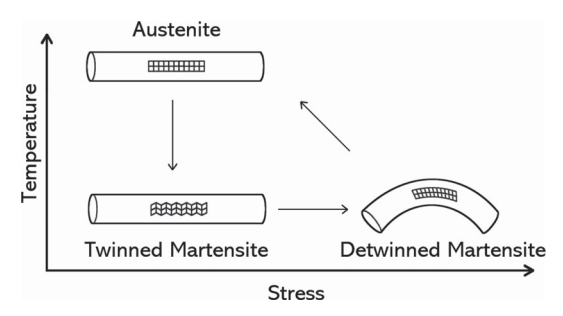


Fig. 2. Phase conversion of SMA.

arranged in a tight pattern, making the SMA more rigid. At low temperature, the SMA is in a martensite phase where the atoms could be rearranged in a loose pattern so that the SMA is more pliable. If no external stress is applied to the SMA, its crystal structure stays in a twinned martensite state, and its overall shape is the same as an austenite phase. If external stress is applied, the SMA crystal structure changes to the detwinned martensite state, and the overall shape is modified according to the stress. Once the SMA returns from detwinned martensite state to austenite state when heated, it returns to its originally predefined shape. From a crystallographic viewpoint, the heat energy leads to the reorientation of SMA atoms to the symmetric pattern. From the microscopic view, this reorientation results in the recovery of the predefined physical shape once it reaches a high temperature. This process of converting from a detwinned martensite state at low temperature to an austenite state at high temperature is irreversible in that an austenite state cannot return to a detwinned martensite state without external stress. Thus, SMA has built-in memory to remember the predefined high-temperature configuration [13]. These unique properties have been used to design various sensors and actuators recently [14]-[18].

In this letter, temperature sensing is achieved using controlled thermo-mechanical training of an SMA as a function of temperature and controlling this process for a given temperature range. This imparts the SMA with a specific and characteristic temperature-sensitive mechanical deformation that can be used for sensing temperature. SMA-based antenna structure is proposed for readout. Detection is achieved remotely by monitoring the radiation intensity or pattern from this SMA-based antenna.

# III. SENSOR DESIGN

Conventional temperature threshold antenna sensors rely on monitoring resonant frequency shifts or impedance change due to the temperature variations [19], [20]. Such approaches require

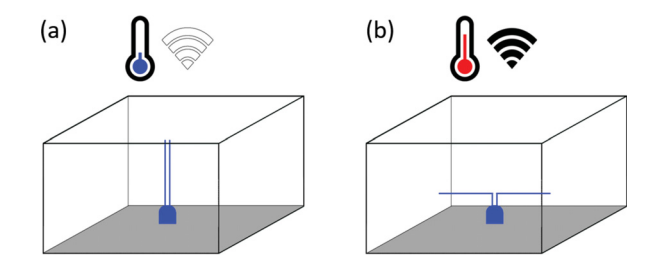


Fig. 3. (a) Antenna is placed in a parallel line configuration at the source when the temperature is below the threshold. The radiation is negligible since the radiation from the parallel lines is mutually canceled (b) If the temperature exceeds the threshold, the configuration changes to a dipole antenna resulting in substantial radiation. The antenna configuration change is irreversible, providing a memory of the event at any time point in the future after the temperature crossing event.

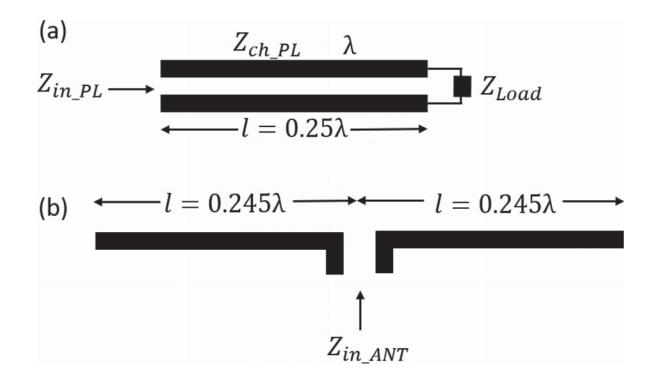


Fig. 4. (a) Parallel line configuration. (b) Dipole antenna configuration.

a vector network analyzer or wireless TX/RX link to detect the spectrum shift to map the impedance variation to temperature, making the readout impractical for economical supply chain visibility. Moreover, based on how the system is implemented, there could be other factors that affect the antenna resonant frequency or the impedance, so calibration is essential before deployment. In the approach proposed here, a reconfigurable SMA-based antenna is designed to maximize the radiation difference between the binary states: below and above the threshold temperature. The antenna is manually deformed into two parallel lines configuration below the threshold temperature as in Fig. 3(a). If the ambient temperature increases above the threshold, the sensor changes to the predefined dipole antenna architecture as indicated in Fig. 3(b). Given the SMA properties reviewed in Section II, this process is irreversible so that the threshold crossing event is recorded within the configuration of the SMA-based antenna.

From the input impedance perspective, the closely placed parallel lines form a transmission line. According to the transmission line theory, the input impedance of parallel lines  $Z_{\text{in\_PL}}$  is determined by the characteristic impedance of the parallel lines  $Z_{\text{ch\_PL}}$ , the load impedance  $Z_{\text{Load}}$ , the feedlines length l, and the wavelength  $\lambda$ , as in the following equation [see Fig. 4(a)]:

$$Z_{\text{in\_PL}} = Z_{\text{ch\_PL}} \frac{Z_{\text{Load}} \cos(\frac{2\pi l}{\lambda}) + j Z_{\text{ch\_PL}} \sin(\frac{2\pi l}{\lambda})}{Z_{\text{ch\_PL}} \cos(\frac{2\pi l}{\lambda}) + j Z_{\text{Load}} \sin(\frac{2\pi l}{\lambda})}.$$
 (1)

By ensuring the length of the transmission line is  $\lambda/4$ , the input impedance of the transmission line  $Z_{\text{in\_PL}}$  is 0 when the load is

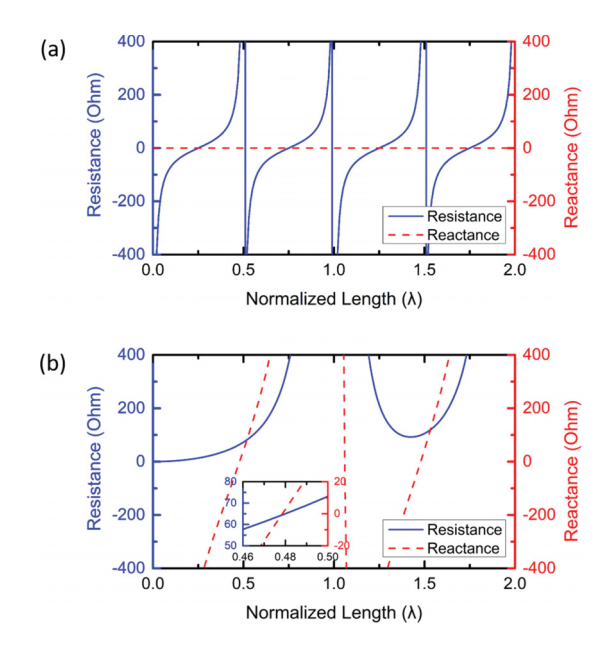


Fig. 5. (a) Impedance of the parallel line. (b) Impedance of the dipole antenna.

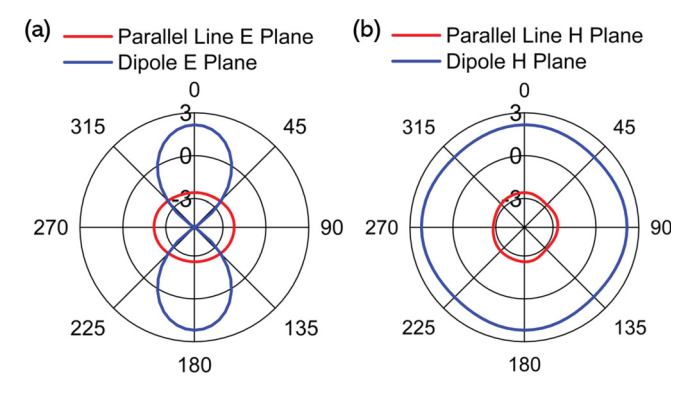


Fig. 6. (a) E-plane radiation of dipole antenna and parallel line. (b) H-plane radiation of dipole antenna and parallel line.

an open condition, as in Fig. 5(a) and the following equation:

$$Z_{\text{in\_PL}} = 0$$
, for  $l = \frac{n\lambda}{4}$ ,  $n = \text{integer}$ . (2)

Therefore, ideally, there is no energy delivered to the parallel lines from the transmitter at this frequency, so the antenna in this condition cannot radiate energy. The dipole antenna input impedance is related to the dipole length as well. The input impedance of a half-wavelength dipole antenna is 73 + j42.5. Its corresponding one leg is a quarter wavelength. If the length is around  $0.49\lambda$  as in Fig. 4(b), then the imaginary part of the input impedance will be zero as in Fig. 5(b). This choice of arm length serves the dual purpose; when in parallel line configuration it delivers low radiation and when in dipole configuration, it delivers maximum radiated power

The radiation pattern of the dipole antenna configuration and parallel line configuration is shown in Fig. 6. The large difference of the radiations from the two configurations provides numerical validation of the proposed concept.

Basically, by design, we ensure that there is a significant difference in the strength and pattern of the radiation for these two configurations. In a parallel line configuration, the radiation is negligible since the fields from two arms cancel each other. Placing the antenna in a dipole configuration yields strong far-field radiation since the fields from the two arms argue each other. This drastic difference in radiation between the two scenarios makes the sensor immune from noise and other sources of mechanical disruption, providing accurate detection of temperature threshold crossing. A commercial radio frequency reader can remotely detect wirelessly even if the sensor is buried inside a package. If the reader fails to communicate with the sensor inside the package, it indicates that the antenna of the sensor remains in parallel line configuration with negligible radiation, so that the package has experienced no temperature threshold crossing. If the reader can sense the radiation, it indicates that the package has experienced a temperature-crossing event during shipping at some point in the past that lead to the antenna to change to the new dipole antenna configuration.

Note that the wireless thermal threshold detection is simple and the threshold temperature sensing and recording rely purely on the natural phase change characteristics of the SMA. There is no need for memory elements to record the event, and there is no other data processing needed such as to compare the resonant frequencies or to measure any backscatter signal strengths of the two temperature conditions. Moreover, it does not need any power source at the sensor end. The whole sensor platform is low-cost and compact, scalable to monitor large number of goods.

### IV. EXPERIMENTAL RESULTS

Commercially available SMA made from an alloy of nickel and titanium is used to realize the SMA-based temperature sensor. The diameter of the wire is 0.5 mm and it has a phase change threshold temperature of 30 °C. Two SMA wires are fixed onto an L-shaped strut and heated to a temperature of 300°C (Fisher Scientific Isotempâ Muffle Furnace 550) for 10 min as in Fig. 7. A high-temperature resistant tape can be used to fix the L-shape. Then, quickly quenched it into cold water. The two steps form the high-temperature predefined L-shaped configuration. A small printed circuit board (PCB) is fabricated for mounting two SMA wires to form the antenna. The SMA wires are soldered into the through-holes of the PCB. To detect the threshold crossing, the antenna shape is predeformed into the parallel line configuration at a temperature below 30°C, as in Fig. 8(a). Once the environment temperature exceeds 30 °C, the parallel lines convert to the dipole antenna configuration within several seconds as in Fig. 8(b). We observe a maximum of 2°C temperature error over 10 tests. The error is mainly from the imbalanced temperature environment surrounding the antenna sensor. The antenna sensor has built-in memory to lock in the antenna configuration even if the temperature drops below the threshold. The simulated and measured  $S_{11}$  of parallel lines configuration and the dipole antenna configuration is in Fig. 8(c). At 900 MHz, the parallel-line configuration shows  $S_{11}$  close to 0 dB for temperature less than the threshold, and -19 dB for temperature above the threshold. The large radiation difference allows any commercial radio frequency reader to differentiate whether the sensor has experienced a threshold-crossing event. This solution has the advantage that the temperature crossing

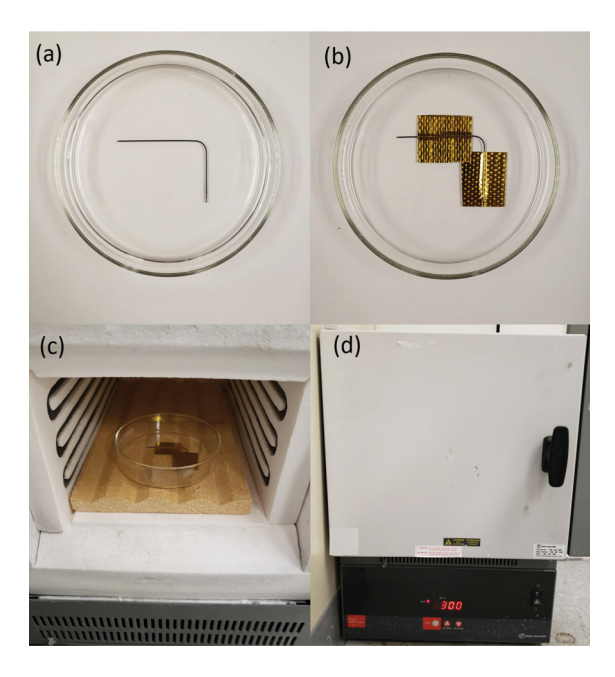


Fig. 7. (a) Fold the SMA wire into L-shape. (b) Fixed the pattern with a high-temperature resilient tape. (c) Bring it into furnace. (d) Heat up to  $300\,^{\circ}$ C for 10 min.

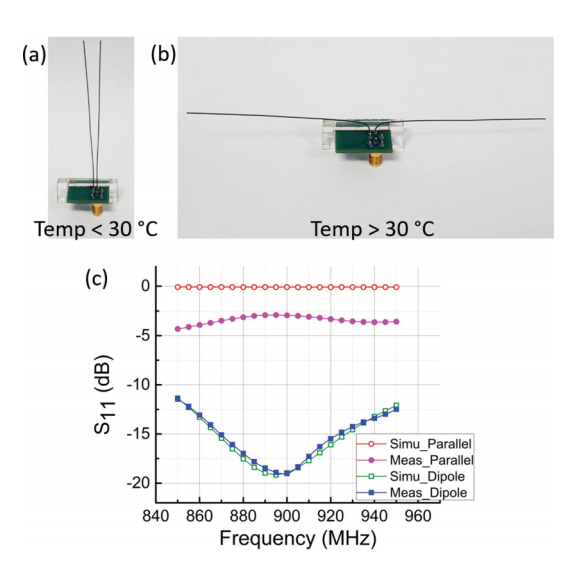


Fig. 8. SMA is deformed at a temperature below the  $30^{\circ}$ C threshold temperature. (b) SMA unfolded the two arms when the ambient temperature exceeds  $30^{\circ}$ C. (c) Simulation (Simu) and measurement (Meas) of one-way SMA-based temperature sensor.

can be deduced without opening the package as shown in Fig. 3, however, access to the antenna port is needed.

The SMA-based antenna can be folded back to the parallel line configuration at a temperature less than the threshold for multiple usages. Note that by choosing SMA with appropriate transition temperature, one can implement a temperature sensor for another value [13]. The accuracy of this sensor is typically limited to  $\pm 1\,^{\circ}\text{C}$ . The error is due to residual hysteresis in SMA and the temperature tolerances on the overall SMA based sensor. However, this is a nonissue in many applications where large error tolerances can be tolerated.

#### V. CONCLUSION

This letter presents a simple battery-free reusable sensor for recording temperature threshold-crossing activity using the natural phase-change property of SMAs. We illustrate how SMA inherently records a temperature-crossing event in its mechanical configuration. The sensor consolidates the temperature sensing, recording, and wireless communication into a single SMA-based antenna. The readout is achieved by constructing a dipole antenna using arms made of SMAs. Given the low cost of the sensor platform, one can apply this to the monitoring of a large number of packages.

## REFERENCES

- K. Biji, C. Ravishankar, C. Mohan, and T. Srinivasa Gopal, "Smart packaging systems for food applications: A review," *J. Food Sci. Technol.*, vol. 52, no. 10, pp. 6125–6135, 2015.
- [2] A. Ra and D. Yadav, "Evaluating wiring configurations for RTD sensor in temperature measurement," *I-Manager's J. Electron. Eng.*, vol. 10, no. 1, pp. 1–8, 2019.
- [3] V. Blay and L. F. Bobadilla, "Numerical study of the accuracy of temperature measurement by thermocouples in small-scale reactors," *Chem. Eng. Res. Des.*, vol. 131, pp. 545–556, 2018.
- [4] W. Yang, H. Jiang, and Z. Wang, "A poly resistor based time domain CMOS temperature sensor with 9b SAR and fine delay line," Sensors, vol. 19, no. 8, p. 2053(1-8), 2019.
- [5] D. Yan et al., "Low-cost wireless temperature measurement: Design, manufacture, and testing of a PCB-based wireless passive temperature sensor," Sensors, vol. 18, no. 2, p. 532(1-14), 2018.
- [6] J. Torres, B. García-Cámara, I. Pérez, V. Urruchi, and J. Sánchez-Pena, "Wireless temperature sensor based on a nematic liquid crystal cell as variable capacitance," *Sensors*, vol. 18, no. 10, p. 3436(1-9), 2018.
- [7] A. Albrecht, J. Salmeron, M. Becherer, P. Lugli, and A. Rivadeneyra, "Screen-printed chipless wireless temperature sensor," *IEEE Sensors J.*, vol. 19, no. 24, pp. 12011–12015, Dec. 2019
- [8] W. Wang, R. Owyeung, A. Sadeqi, and S. Sonkusale, "Single event recording of temperature and tilt using liquid metal with RFID tags," *IEEE Sensor J.*, vol. 20, no. 6, pp. 3249–3256, Mar. 2020
- [9] W. Wang, W. Zeng, W. Ruan, E. Miller, and S. Sonkusale, "Thermomechanically trained shape memory alloy for temperature recording with visual readout," *IEEE Sensors Lett.*, early access, Dec. 14, 2020, doi: 10.1109/LSENS.2020.3044294.
- [10] W. Wang, A. Sadeqi, and S. Sonkusale, "All-around package security using radio frequency identification threads," in *Proc. IEEE Sensor*, 2018, pp. 1–4
- [11] W. Wang, A. Sadeqi, H. Nejad, and S. Sonkusale, "Cost-effective wireless sensors for detection of package opening and tampering," *IEEE Access*, vol. 8, pp. 117122–117132, 2020
- [12] C. Asci, W. Wang, and S. Sonkusale, "Security monitoring system using magnetically-activated RFID tags," in *Proc. IEEE Sensors*, 2020, pp. 1–4.
- [13] J. Jani, M. Leary, A. Subic, and M. Gibson, "A review of shape memory alloy research, applications and opportunities," *Mater. Des.*, vol. 56, pp. 1078–1113, 2014.
- [14] C. R. Knick, D. J. Sharar, A. A. Wilson, G. L. Smith, C. J. Morris, and H. A. Bruck, "High frequency, low power, electrically actuated shape memory alloy MEMS bimorph thermal actuators," *J. Micromech. Micro-eng.*, vol. 29, no. 7, 2019, Art. no. 075005.
- [15] Y. Kim et al., "Bidirectional rotating actuators using shape memory alloy wires," Sensors Actuators A: Phys., vol. 295, no. 15, pp. 512–522, 2019
- [16] M. R. A. Kadir, D. E. OctorinaDewia, M. NajebJamaludin, M. Nafea, and M. S. M. Ali, "A multi-segmented shape memory alloy-based actuator system for endoscopic applications," *Sensors Actuators A: Phys.*, vol. 296, no. 1, pp. 92–100, 2019
- [17] L. Meng *et al.*, "A mechanically intelligent crawling robot driven by shape memory alloy and compliant bistable mechanism," *J. Mech. Robot.*, vol. 12, no. 6, 2020, Art. no. 061005.
- [18] H. Yin, L. Tian, and G. Yang, "Design of fibre array muscle for soft finger with variable stiffness based on nylon and shape memory alloy," *Adv. Robot.*, vol. 34, no. 9, pp. 599–609, 2020.
- [19] Y. Shafiq *et al.*, "A reusable battery-free RFID temperature sensor," *IEEE Trans. Antennas Propag.*, vol. 67, no. 10, pp. 6612–6626, Oct. 2019
- [20] A. Lazaro, A. Ramos, D. Girbau, and R. Villarino, "Signal processing techniques for chipless UWB RFID thermal threshold detector detection," *IEEE Antennas Wireless Propag. Lett.*, vol. 15, pp. 618–621, 2016.